Indian Journal of Chemistry
Vol. 61, May 2022, pp. 528-536

Synthesis, structure, Hirshfeld surface, crystal voids, energy framework and DFT analysis of 1*H*-benzo[d]imidazole-2(3*H*)-thione

M Singh[a], S Anthal[b], Kamal[c], M B Deshmukh[d] & Rajni Kant[a]*

[a] Department of Physics, University of Jammu, Jammu 180 006, India
[b] Department of Physics, Government Degree College, Udhampur 182 101, India
[c] Department of Chemistry, Indian Institute of Technology, Jammu 181 221, India
[d] Department of Chemistry, Shivaji University, Kolhapur 416 004, India
E-mail: rkant.ju@gmail.com

Received 11 July 2021; accepted (revised) 22 April 2022

1*H*-Benzo[d]imidazole-2(3*H*)-thione (BIT), ($C_7H_6N_2S$), has been synthesized and characterized by IR, ^{1}H NMR, EI-MS mass spectra, single crystal X-ray data and elemental analysis techniques. The final refinement of the structure yielded R-facor of 4.2%. for 651 observed reflections. The structure has been characterized for its interesting properties like Hirshfeld surface analysis which has been carried out to understand different interaction contacts of the molecule and strength of the molecular packing in the crystal. The mechanical strength of crystal has been confirmed from a void volume analysis. The energy frameworks have been constructed for the investigation of stability of the compound and the type of dominant energy through different intermolecular interaction energies. Density functional theory (DFT) calculations have been performed to analyze Mulliken charge and HOMO-LUMO energy levels. An integrated approach for the crystal structure and its properties analyses are presented in this paper.

Keywords: Crystal structure, X-ray diffraction, direct methods, Hirshfeld surface, crystal voids, energy framework, DFT calculations

Benzimidazoles are classes of heterocycles that are of considerable interest because of the diverse range of their biological properties. Among a wide variety of nitrogen heterocycles that have been explored for developing pharmaceutically important molecules, benzimidazole derivatives have found diverse therapeutic applications[1-4]. These are biologically important scaffolds mostly useful as structural motif for the development of pharmaceutical or biological molecules. Though the crystal structure of BIT has already been reported[5,6], yet we decided to undertake a systematic analysis of its synthesis *via* different route, redetermination of its crystal structure only to investigate the (i) feasibility of intermolecular hydrogen bond interactions that form distinct type of aesthetic supramolecular assemblies in the solid state (ii) Hirshfeld surface (HS), (iii) crystal voids, (iv) Energy framework analysis and (v) quantum chemical aspects to reflect on some interesting properties of this material.

The single crystal X-ray structure analysis of BIT was performed to identify the crystalline phases present in the synthesized compound. The molecular Hirshfeld surface (HS) analysis revealed the differences and similarities of Benzimidazole molecule in the crystal structure. Crystal voids and Energy framework calculations were performed using Crystal Explorer (17.5)[7]. The quantum chemical calculations were carried out by using Density Functional theory (DFT) employing B3LYP/6-311G (d, p) basis set to calculate optimized geometry and atomic charges in the ground state using Gaussian09W[8]. Highest occupied molecular orbital (HOMO) and lowest occupied molecular orbital (LUMO) analysis illuminates information regarding charge transfer within the molecule. Related molecular properties such as ionization potential, electron affinity, global hardness, electronic chemical potential and global electrophilicity of the optimized structure have also been reported.

Abbreviations: BIT- 1*H*-Benzo[d]imidazole-2(3*H*)-thione; SCXRD- single crystal X-ray data; DFT- Density Functional Theory; HOMO- Highest occupied molecular orbital; LUMO- Lowest unoccupied molecular orbital; HS- Hirshfeld surface; CIF- Crystal information report; HF- Hartree-Fock

Experimental Section

Materials and Methods

IR spectra were recorded on JASCO Spectrometer with scanning from 4000 to 450 cm^{-1}. The ^{1}H NMR

on Bruker 300 AVANCE II in DMSO-d6 as a solvent and tetramethyl silane (TMS) as an internal standard. Mass spectra were recorded on Agilent 6540 a Performa spectrometer equipped with an electron spray ionization interface.

Synthesis

The mixture of *o*-phenylenediamine (1.08g., 0.01 mole) and thiocarbonylchloride (1.15g., 0.01mole) in benzene (10 mL) to which two drops of triethyl amine were added and the same reaction mixture refluxed on an oil bath for four hours, then cooled . The solvent was removed under vacuum to get a solid recrystallized from ethanol, yield 70 %, m.p. 300°C. The chemical structure of the compound is shown in Figure 1.

Spectral Data

IR (KBr) : *v* max, 3299-3350 (NH), 1600(C=C), 1265-1072(C=S) cm^{-1}.

^{1}H NMR (DMSO-d6): δ, 12.20 (2H,s exchangeable with D_2O, 2 × NH), 7.10 (2H,d J=7.5 Hz, aromatic protons), 7.19(2H,d J=7.5 Hz, aromatic protons) ppm.

Mass(EI-MS): m/z, 150

X-ray crystallography

Crystal Structure Determination and Refinement

Single crystal X-ray diffraction data were obtained from Bruker D8 Venture using a multilayer mirror optics monochromator and a MoKα rotating-anode X-ray tube of wavelength (λ = 0.71073 Å). The structure was solved by direct methods using SHELXS97 [9] and SHELXL97 [10] software packages. The crystallographic data are summarized in Table I. All the hydrogen atoms were fixed geometrically and allowed to ride on the corresponding non-H atoms with U_{iso}(H) = 1.2 U_{eq}(N) and 1.2 U_{eq}(C) (N-H= 0.86 Å, C-H= 0.93 Å). The final refinement cycles converged to an R-factor of 0.0422 and *w*R(F^2) = 0.1300 for 651 observed reflections. Residual electron densities range from -0.34 to 0.30 e.$Å^{-3}$. Atomic scattering factors were taken from International Tables for X-ray Crystallography (1992, Vol. C, Tables- 4.2.6.8 and 6.1.1.4). The Geometry of the molecule was calculated using the WinGX[11], PARST[12], PLATON[13] and MERCURY[14] software.

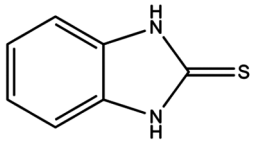

Figure 1 — Chemical structure of 1H-Benzo[d]imidazole-2(3H)-thione

Computational Details

The Hirshfeld surface (HS) mapped plots (d_{norm}, 2-D fingerprint, shape-index and curvedness) and unit cell voids were generated using Crystal-Explorer package (ver.17.5)[7]. Energy framework analysis explores the intermolecular interaction energies between the molecules of the cluster within 3.8Å and these calculations were performed using the Crystal explorer with B3LYP function and 6-31G (d, p) basic set[7]. The calculations for 1H-Benzo[d]imidazole-2(3H)-thione were carried out by using Hartree-Fock (HF) and Density Functional theory (DFT) methods with Gaussian 09W[8]. The molecular geometry was optimized by HF theory and subsequently re-optimized by DFT using standard B3LYP/6-311G (d, p) basis sets. DFT calculations yielded optimized geometry, bond lengths, bond angles, atomic charges and HOMO–LUMO at standard B3LYP 6-311G (d, p) basis set for the molecule in the ground state by using Gaussian 09W. All the atomic coordinates were imported from the final validated crystal information report (CIF) to Crystal Explorer (17.5) and Gaussian software.

Table I — Crystal data and experimental details

Empirical formula	$C_7H_6N_2S$
Formula weight	150.20
Temperature (K)	293(2)
Crystal system	Monoclinic
Space group	$P2_1/m$
a (Å)	4.9218(7)
b (Å)	8.5610(2)
c (Å)	8.3086(2)
α (°)	90
β (°)	91.755(8)
γ (°)	90
Volume ($Å^3$)	349.92(1)
Z	2
ρ calc (g/cm^3)	1.426
μ (mm^{-1})	0.375
F(000)	156.0
Crystal size (mm^3)	0.12 × 0.08 × 0.06
Radiation	MoKα (λ = 0.71073 Å)
2Θ range for data collection (°)	4.142 to 25.983
Index ranges	$-6 \le h \le 5, -10 \le k \le 10, -10 \le l \le 10$
Reflections collected	8110
Independent reflections	689 [Rint = 0.0429, Rsigma = 0.0429]
Data / restraints / parameters	689 / 0 / 50
Goodness-of-fit on F2	1.288
Final R indexes [I≥2σ (I)]	R1 = 0.0422, wR2 = 0.1299
Final R indexes [all data]	R1 = 0.0439, wR2 = 0.1340
Largest diff. peak /hole (e.$Å^{-3}$)	0.297/-0.342

Result and Discussion

Crystal Structure Analysis

The X-ray crystallographic analysis reveals the existence of half-molecule in the asymmetric unit, with a mirror plane passing through S and C4 atoms. The remaining half fragment of the structure was generated to close the structure. The bond distances, bond angles and torsion angles between the non-H atoms are listed in Table II. The bond angles in the imidazole ring are in good agreement with those existing in imidazole[15,16] and related substituted imidazoles[17]. The sulphur-carbon bond length (1.684(3)Å) is slightly shorter than the nucleoside containing benzimidazole (1.693(4)Å)[18] but agrees well with that of 1-methyl-1*H*-benzimi dazole-2(3*H*)-thione (1.684(2)Å)[19]. In imidazole ring, slight difference in bond lengths is attributed to the delocalization of the imidazole electron density. Thus, the N1-C4 bond length (1.356(2)Å) is closer to partial C-N bond [single C-N bond 1.47Å and double C-N bond 1.27Å][20] and the N1-C3 = 1.384(2) is shorter than a C-N bond length. The pairs of molecules form dimers (Figure 2) *via* N-H…S hydrogen bond (where N act as a donor to S, Table III) which eventually result in the construction of R_2^2 (8) graph set motif[21].

Table II — Bond distances (Å), Bond angles (°) and Torsion angles (°)

Bond	Distance (Å)	Bond	Distance (Å)
S-C4	1.684(3)	C3-C3'$^{(i)}$	1.392(4)
N1-C4	1.356(2)	C2-C1	1.383(3)
N1-C3	1.387(2)	C1-C1'$^{(i)}$	1.382(5)
C3-C2	1.385(3)		
Bond	**Angles (°)**	**Bond**	**Angles (°)**
C4-N1-C3	110.70(17)	N1'$^{(i)}$-C4-S	126.94(11)
C2-C3-N1	132.24(18)	N1-C4-S	126.94(11)
C2-C3-C3'$^{(i)}$	121.52(12)	C1-C2-C3	116.7(2)
N1-C3-C3'$^{(i)}$	106.24(10)	C1'$^{(i)}$-C1-C2	121.82(13)
N1'$^{(i)}$-C4-N1	106.1(2)		
Bond	**Torsion Angles (°)**	**Bond**	**Torsion Angles (°)**
C4-N1-C3-C2	-179.66(19)	N1-C3-C2-C1	179.70(19)
C4-N1-C3-C3'$^{(i)}$	0.83(15)	C3'$^{(i)}$-C3-C2-C1	-0.8(2)
C3-N1-C4-N1'$^{(i)}$	-1.3(2)	C3-C2-C1-C1'$^{(i)}$	0.8(2)
C3-N1-C4-S	179.14(15)		

Symmetry code: (i) x, -y+1/2, z.

Table III — Hydrogen bonding geometry (e.s.d.`s in parentheses)

D–H…A	D–H(Å)	H…A(Å)	D…A(Å)	D–H…A(°)
N1-H3…S$^{(i)}$	0.86	2.56	3.3714(16)	158

Symmetry codes: (ii) 1-x,-1/2+y,-z

Hirshfeld Surface Analysis

To analyze the intermolecular interaction and packing modes of the molecule in crystalline phase, the Hirshfeld surfaces (HS) divide the crystal space into smooth, non-overlapping, interlocking molecular volumes. The HS and their related 2D fingerprint plots generated using the Crystal-Explorer 17.5[7] were mapped over the normalized contact distance (d_{norm}) (Figure 3) by

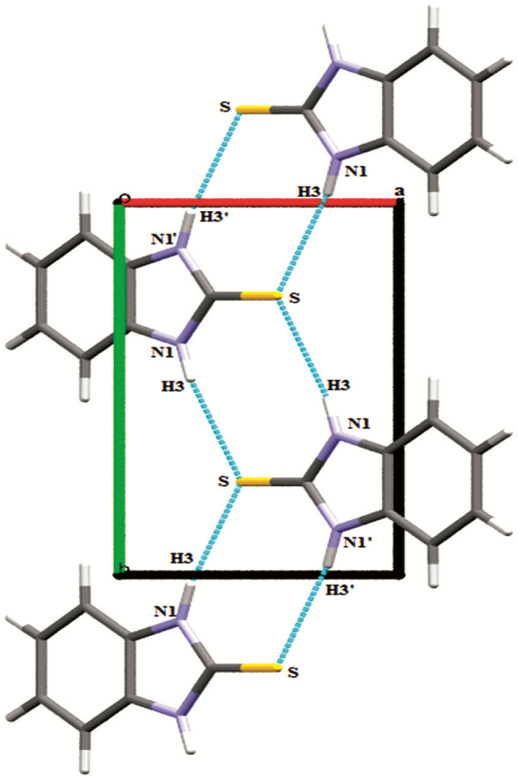

Figure 2 — Molecular plot showing the formation of R_2^2 (8) dimer ring

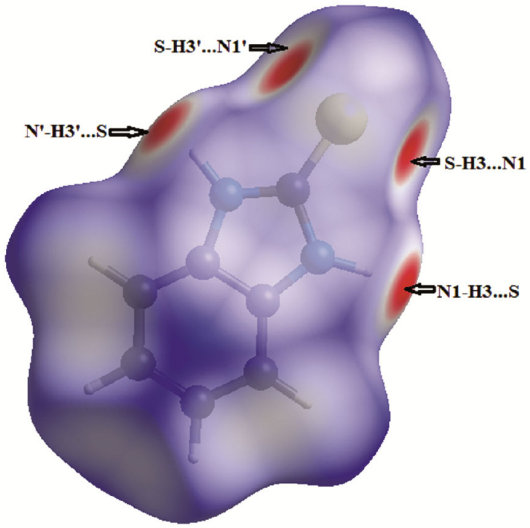

Figure 3 — Hirshfeld surface mapped over $d_{norm.}$

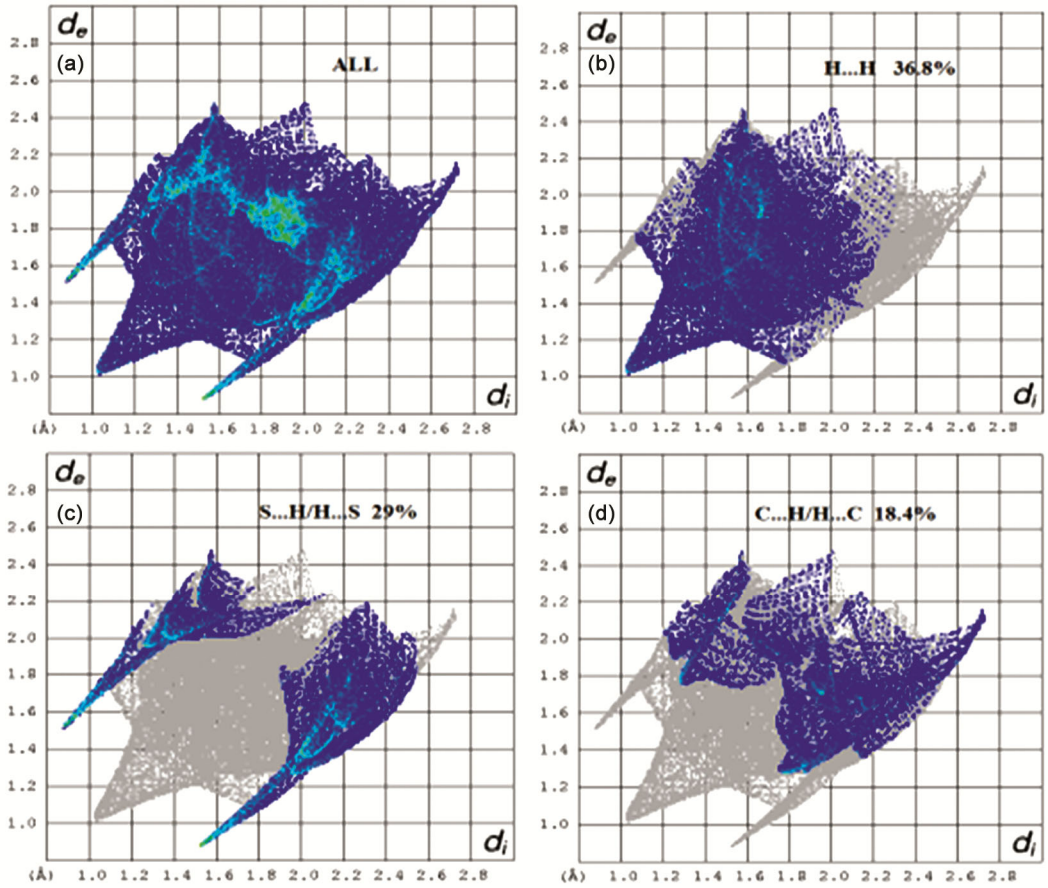

Figure 4 — 2D fingerprint plot of the compound **(a)** From all the contacts, **(b)** Disintegrate fingerprint plot showing H…H (36.8%) contacts, **(c)** S…H/H…S (29%) contacts and **(d)** C…H/H…C (18.4%) contacts

using a white, red and blue color scheme. White color region on the surface represent the contacts equal to the van der waals radii, red and blue colors represent the shorter and longer intermolecular contacts of the molecules, respectively. The four bright red spots as appear on the HS indicates the existence of short hydrogen bond interactions due to S-H…N and N-H…S contacts which are shorter than van der Waals radii.

Figure 4 represents the related fingerprint plot of BIT, created in the d_{norm} range, -0.3319 Å to 1.3327 Å. The parameters di and de (di and de is the distance from the HS to the nearest nucleus inside and outside the surface, respectively) used in the fingerprint plots represent the distances from the HS to the nearest nucleus inside and outside the surface, respectively. For any given pairs of di and de, the white color indicates no occurrence, blue color represents some occurrence and green shows more frequent occurrence. These 2D fingerprint plots give the percentage contribution of each type of contacts to the total HS area. The major contribution to the total HS

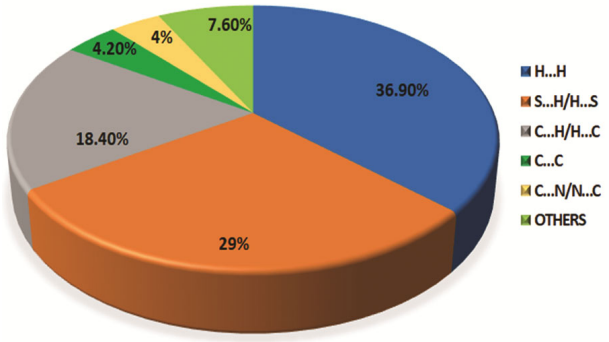

Figure 5 — The relative contributions (%) for a variety of contacts in the crystal structure

area is H…H contacts with 36.90 % while the remaining significant contributions are from S…H/H…S (29%) and C…H/H…C (18.40%). The extended symmetrical spikes in Figure 4(c) are the characteristics of S…H/H…S intermolecular interaction while spikes in Figure 4(b) and (d) are due the interaction of H…H and C…H/H…C, respectively. Figure 5 contains the relative percentage

of contributions for a variety of contacts in the crystal structure.

Shape Index and Curvedness

The study of HS reveals more details about the shape and molecular packing in the crystal such as shape index and curvedness. Figure 6(a) represents the mapping over the shape index of the compound BIT. Pairs of red and blue regions on the shape index show the area of touching points of two HS and the red concave regions on the map is around the acceptor atoms and the surface around the donor atoms is shown as blue bumps region[22]. By visualizing the map of shape index it is found that there are no adjacent red and blue triangles; thus suggesting the absence of π … π interaction. Figure 6(b) represents HS mapped over curvedness where large green region (relatively flat) is separated by dark blue boundaries (large positive curvatures). The absence of flat surface patches on the curvedness plot clearly rules out planner stacking between the molecules.

Crystal Voids

Crystal voids are defined as the region of empty space between the molecules in the crystal and this empty space is the region which lies outside the normal van der Waals surface area of molecules in the unit cell within which no nuclei exist. Voids in the crystal structure (as shown in Figure 7 along a and c-axis) are built on the sum of spherical atomic electron densities at the appropriate nuclear positions (procrystal electron density). Based on isosurfaces of the procrystal electron density, the sum of spherical atomic electron densities located at the appropriate nuclear positions[23]. The crystal-voids have been visualized by generating (0.002 au)-isosurface of procrystal electron density. This 0.002 au electron density isosurface contain more than 98% of the electronic charge of molecules and recognize the empty space in crystal by determining the shape and size of molecules. The volume of void comes out to be 31.46 $Å^3$ while the unit cell volume is 349.92$Å^3$ (Table I). With porosity, the calculated void volume is about 9% that is why there are no large cavities. We note that 0.002 au electron-density isosurface are not completely closed around the components, but are open at those locations where interspecies approaches are found, *e.g.* S-H3…N1.

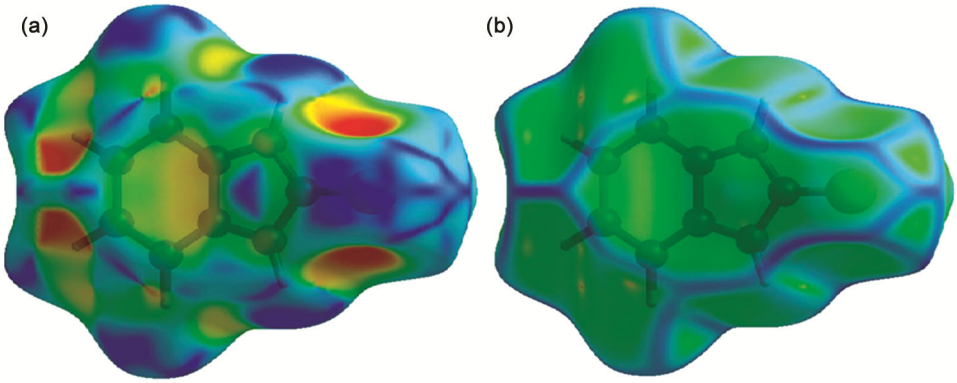

Figure 6 — **(a)** Shape index and **(b)** curvedness plot mapped onto the Hirshfeld surface

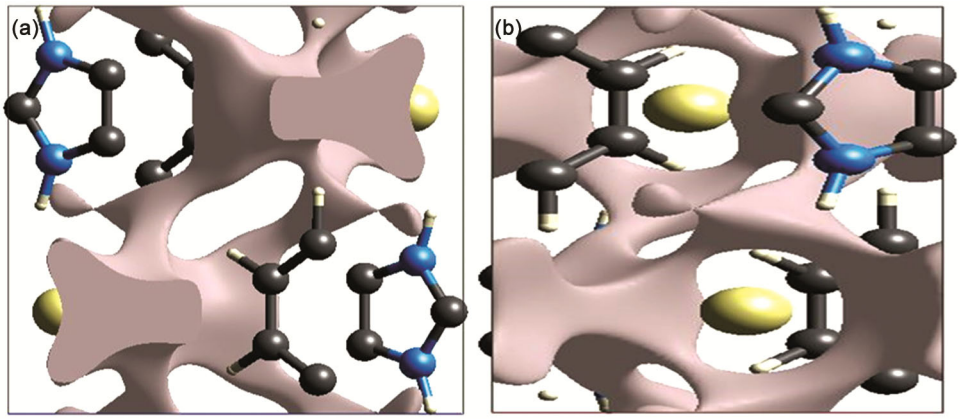

Figure 7 — Unit cell void at (0.002 au)-isosurface along **a** and **c**-axis

Energy Framework

The analysis of energy frameworks is used to explore the intermolecular interaction energies between the molecules of the cluster within 3.8 Å around a single molecule of BIT. These calculaions were carried out using Crystal Explorer (17.5) at B3LYP/3-21G basic set[7]. The scale factors used for the construction of energy framework for B3LYP/6-31G (d, p) electron densities are k_ele = 1.057, k_pol = 0.740, k_disp = 0.871, k_rep = 0.618[24]. Table IV lists the interaction energies, *viz*. electrostatic (E_ele = -97.3 kJ/mol), polarization (E_pol = −25.8 kJ/mol), dispersion (E_dis = −86.2 kJ/mol) and repulsion (E_repl = 121.2 kJ/mol). The total interaction energy is -118.1 kJ/mol. The electrostatic energy dominates over dispersion energies framework. In Figure 8 images of different interactions energies – coulomb interaction energy (red), dispersion energy (green) and total energy (blue) are shown along c-axes. The cylinders shown in energy framework represent the relative strengths of molecular packing in different directions. In the energy framework, an overall scale factor is applied to expand or contract the size of the cylinders[25]. The weak interactions were omitted below certain threshold energy only to make the figure less crowded.

Molecular Geometry

Figure 9 represents an optimized structure and its structural parameters calculated using HF and DFT methods [HF/6-311G (d, p) and B3LYP/6-311G (d, p)] are presented in Table IV and VI, respectively[8]. The optimized parameters indicate a close match with the experimental data. The largest difference between experimental and calculated bond length N1-C3 by B3LYP is about 0.0019 Å as presented in Table V. Some of the bond lengths increase from HF to B3LYP level. The bond angles C4-N1-C3, C2-C3-N1, N1-C4-S, N1'-C4-S, C1-C2-C3 and C1'-C1-C2 increases from HF level to B3LYP level and the remaining bond angles decreases from HF level to B3LYP level as presented in Table VI. The global minimum energy acquired for structure optimization of the title compound is -775.11601012 au and -778.19949730 au, respectively. The difference between these two energy values is about -3.08 au.

Atomic Mulliken Charge

Atomic charges in a molecule are linked to dipole moment, electronic structure, molecular polarizability and other properties of the molecule. The atomic charge values have been derived by the Mulliken population analysis[26]. The net atomic charges of the

Table IV — Interaction energy (kj/mol) of the compound BIT

N	Symop	R	Electron Density	E_ele	E_pol	E_dis	E_rep	E_tot
2	x, y, z	4.92	B3LYP/6-31G(d,p)	-2.3	-3.4	-27.6	19.4	-17.1
2	-x, y+1/2, -z	6.31	B3LYP/6-31G(d,p)	-71.9	-14.6	-14.3	68.1	-57.1
2	-x, y+1/2, -z	7.19	B3LYP/6-31G(d,p)	-2.1	-0.7	-12.8	8.9	-8.4
2	x, y, z	9.79	B3LYP/6-31G(d,p)	-4.7	-1.3	-4.0	3.1	-7.5
2	-x, y+1/2, -z	5.19	B3LYP/6-31G(d,p)	-10.2	-4.9	-18.3	12.9	-22.4
2	-x, y+1/2, -z	9.48	B3LYP/6-31G(d,p)	0.8	-0.6	-8.0	8.8	-1.2
2	x, y, z	8.56	B3LYP/6-31G(d,p)	5.3	-0.3	-1.2	0.0	4.4

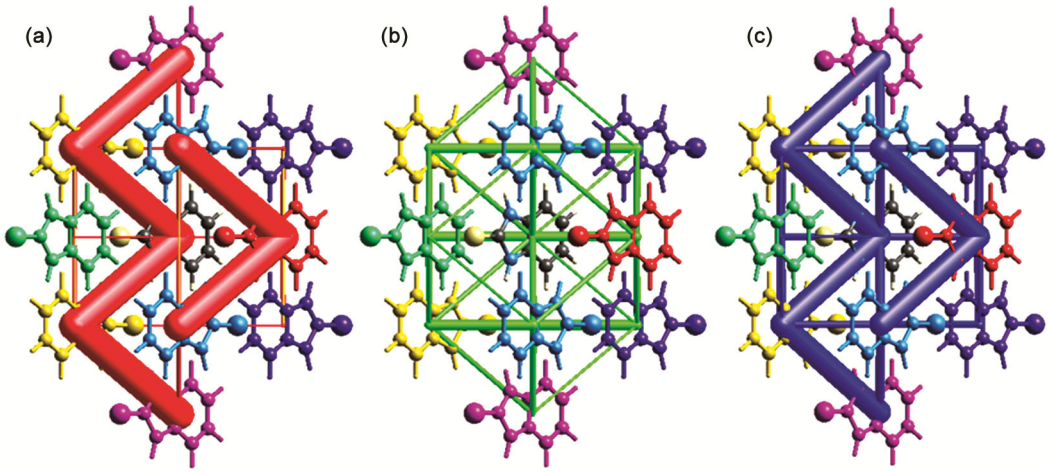

Figure 8 — Energy framework of BIT along c-axis **(a)** Coulomb energy, **(b)** dispersion energy and **(c)** total energy

DFT optimized structure were calculated at HF/6-311 G (d, p) and B3LYP/6-311 G (d, p) basis set using Gaussian 09 software and are tabulated in Table VII[8]. In the present work, the magnitudes of atomic charges of hydrogen atoms decrease from HF to DFT level of calculations and these hydrogen atoms exhibit positive charges. The asymmetric unit present in the compound BIT contains one-half molecule, in which a mirror plane passes through S and C4 atoms. The value of Mulliken charges for S is -0.322 and -0.241 at HF/6-311 G (d, p) and B3LYP/6-311 G (d, p) basis sets, respectively. The atomic charges on C4, C3 and C3' atoms exhibit positive charges in both the cases whereas the remaining carbon atoms are negatively charged. The atoms such as N1 and N1', C1 and C1', C2 and C2', C3 and C3', H1 and H1', H2 and H2' have the same values of atomic Mulliken charges as they are the mirror images of each other.

Frontier Molecular Orbital Analysis

The energies of highest occupied molecular orbital (HOMO) and lowest occupied molecular orbital (LUMO) are very beneficial for physicists and chemists and are very significant terms in quantum chemistry[27]. The HOMO depicts an ability to donate an electron whereas the LUMO describes the ability to gain an electron. The HOMO-LUMO energies plot is given in Figure 10. The HOMO is located at -5.69 eV over the entire molecule whereas LUMO is at -1.12 eV which presents that charge transfers occur within the molecule. The energy difference between the HOMO and LUMO orbital is 4.57 eV and this difference is called HOMO-LUMO gap that is an important stability for structures. This energy gap

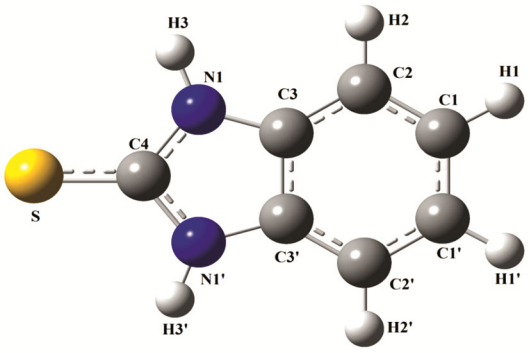

Figure 9 — Optimized structure of compound BIT

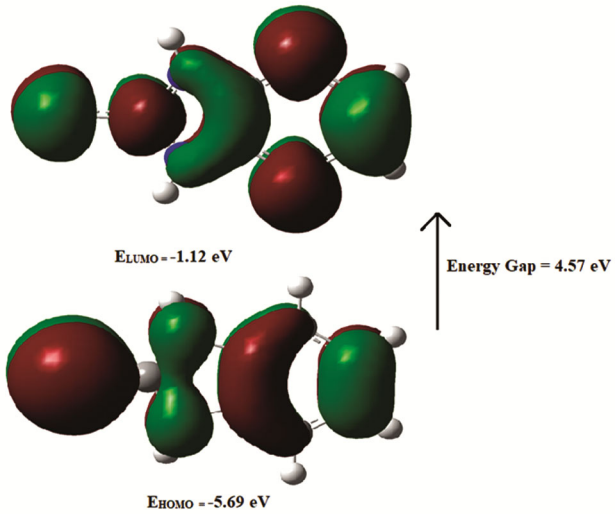

Figure 10 — HOMO-LUMO plot of compound BIT

Table V — Calculated Bond lengths (Å) of the molecule with HF and DFT theory employing 6-311 G(d,p) basis set.

Atom no.	XRD data	HF/6-311G(d,p)	DFT/6-311G(d,p)
S-C4	1.684	1.670	1.667
N1-C4	1.356	1.348	1.375
N1-C3	1.387	1.388	1.389
C3-C2	1.385	1.388	1.407
C3-C3'	1.392	1.378	1.388
C2-C1	1.383	1.387	1.396
C1-C1'	1.382	1.389	1.398

Table VI — Calculated Bond angle (°) of the molecule with HF and DFT theory employing 6-311 G(d,p) basis set

Structural Parameters	XRD data	HF/6-311G(d,p)	DFT/6-311G(d,p)
C4-N1-C3	110.70	111.11	111.65
C2-C3-N1	132.24	132.50	132.63
C2-C3-C3'	121.52	121.54	121.32
N1-C3-C3'	106.23	105.96	106.05
N1-C4-N1'	106.10	105.86	104.60
N1-C4-S	126.94	127.07	127.70
N1'-C4-S	126.94	127.07	127.70
C1-C2-C3	116.70	117.18	117.34
C1'-C1-C2	121.82	121.28	121.34

Table VII — Atomic charges for optimized geometry of the compound BIT

Atom no.	HF/6-311 G(d,p)	B3LYP/6-311 G(d,p)
S	-0.322	0.241
C4	0.264	0.139
N1	-0.514	-0.410
N1'	-0.514	-0.410
C3	0.201	0.148
C3'	0.201	0.148
C2	-0.053	-0.046
C2'	-0.053	-0.046
C1	-0.099	-0.103
C1'	-0.099	-0.103
H1	0.107	0.101
H1'	0.107	0.101
H2	0.106	0.100
H2'	0.106	0.100
H3	0.280	0.260
H3'	0.280	0.260

Table VIII — HOMO-LUMO and other related molecular properties of the compound BIT

Molecular parameters (eV)	B3LYP/6-311G(d,p)
E_{LUMO}	−1.12
E_{HOMO}	−5.69
E_{LUMO} - E_{HOMO}	4.57
Ionization potential (I)	5.69
Electron affinity (A)	1.12
Electronegativity ($\varkappa$)	3.40
Global hardness (η)	2.28
Chemical potential (μ)	−3.40
Global electrophilicity (ω)	2.54

describes the eventual charge transfer interaction within the molecule. The energy of the HOMO is directly proportional to the ionization potential ($I = -E_{HOMO}$) whereas the energy of the LUMO is directly proportional to the electron affinity ($A = -E_{LUMO}$)[28]. The hardness of the molecule corresponds to the gap between the HOMO and LUMO orbital energies. The larger the HOMO-LUMO energy gap the harder the molecule whereas the smaller energy gap represents the high reactivity and low stability of the molecule. The global hardness, $\eta = 1/2\ (E_{LUMO} - E_{HOMO})$. The hardness has been related with the stability of chemical system. The electron affinity can be used in combination with ionization energy to calculate chemical potential, $\mu = 1/2\ (E_{LUMO} + E_{HOMO})$. The global electrophilicity index, $\omega = \mu^2/2\eta$ is also calculated and all these molecular properties above are given in Table VIII.

Conclusions

The compound 1H-Benzo[d]imidazole-2(3H)-thione was synthesized and characterized by IR, ^{1}H NMR and EI-MS mass spectral techniques. The crystallographic structure was obtained by using X-ray diffraction method. The structure is reinforced by N-H…S intermolecular hydrogen bond. The molecular HS and 2D fingerprint plots were analyzed to know the intermolecular interaction contacts and the percentage contribution of each type of contact. The major contribution is from H-H contacts with 36.90%. Further, the void volume (9% of total unit cell volume) also confirms that grown crystal is hard. The energy frameworks studies reveal out the significant contributions of electrostatic compound in the title compound BIT. Further, we have thoroughly examined the molecular structure, atomic Mulliken charges, HOMO-LUMO energy gaps and other molecular properties of the optimized geometry of the 1H-Benzo[d]imidazole-2(3H)-thione molecule by using DFT theory using B3LYP/6-311G (d, p) basis set. Optimized geometry parameters compared to the reported X-ray crystallographic data, which showed a good agreement with each other. The HOMO-LUMO analysis imparted the stability of the compound as well as the charge transfer within the molecule.

Acknowledgements

Rajni Kant is thankful to the University of Jammu for financial assistance received under RUSA- 2.0 Project of Government of India.

Reference

1 Bauer J, Kinast S, Burger-Kentischer A, Finkelmeier D, Kleymann G, Rayyan W.A, Schroppel K, Singh A, Jung G, Wiesmuller K H, Rupp S & Eickhoff H J, *Med Chem*, 54 (2011) 6993.
2 Garudachari B, Satyanarayana M N, Thippeswamy B, Shivakumar C K, Shivananda K N, G. Hegde G & Isloor A M, *Eur J Med Chem*, 54 (2012) 900.
3 Mizuno C S, Chittiboyina A G, Shah F H, Patny A, Kurtz T W, Pershadsingh H A, Speth R C, Karamyan V T, Carvalho P B & Avery M A, *J Med Chem*, 53 (2010) 1076.
4 Patel R V, Patel P K, Kumari P, Rajani D P & Chikhalia K H, *Eur J Med Chem*, 53 (2012) 41.
5 Wang D-C, Mi S, Xu W, Jiang L, & Huang X-M, *Acta Crystallographica Section E: Structure Reports Online*, 65 (2009) o756.
6 Ravikumar K, Mohan K C, Bidyasagar M & Swamy G Y S K, *J Chem Crystallogr*, 25 (1995) 325.
7 Turner M J, Mckinnon J J, Wolff S K, Grimwood D J, Spackman P R, Jayatilaka D & Spackman M A, Crystal Explorer 17.5, The University of Western Australia (2017).
8 Frisch M J, Trucks G W, Schlegel H B, Scuseria G E, Robb M A, Cheeseman J R, Scalmani G, Barone V, Mennucci B, Petersson G A, Nakatsuji H, Caricato M, Li X, Hratchian H P, Izmaylov A F, Bloino J, Zheng G, Sonnenberg J L, Hada M, Ehara M, Toyota K, Fukuda R, Hasegawa J, Ishida M, Nakajima T, Honda Y, Kitao O, Nakai H, Vreven T, Montgomery Jr J A, Peralta J E, Ogliaro F, Bearpark M, Heyd J J, Brothers E, Kudin K N, Staroverov V N, Kobayashi R, Normand J, Raghavachari K, Rendell A, Burant J C, Iyengar S S, Tomasi J, Cossi M, Rega N, Millam N J, Klene M, Knox J E, Cross J B, Bakken V, Adamo C, Jaramillo J, Gomperts R, Stratmann R E, Yazyev O, Austin A J, Cammi R, Pomelli C, Ochterski J W, Martin R L, Morokuma K, Zakrzewski V G, Voth G A, Salvador P, Dannenberg J J, Dapprich S, Daniels A D, Farkas O, Foresman J B, Ortiz, Cioslowski J & Fox D J, Gaussian 09, Revision **A.1**, Gaussian, Inc., Wallingford, CT (2013).
9 Sheldrick G M, *Acta Cryst*, A64 (2008) 112.
10 Sheldrick G M, *Acta Cryst*, C71 (2015) 3.
11 Farrugia L J, *J Appl Crystallogr*, 32 (1999) 837.
12 Nardelli M, *J Appl Crystallogr*, 28 (1995) 659.
13 Spek L, *Acta Crystallogr*, D65 (2009) 148.
14 Macrae C F, Bruno I J, Chisholm J A, Edgington P R, McCabe P, Pidcock E, Rodriguez-Monge L, Taylor R, Streek J V D & Wood P A, *J Appl Cryst*, 41 (2008) 466.
15 McMullan R K, Epstein J, Ruble J R & Craven B M, *Acta Cryst*, B35 (1979) 688.
16 Martinez-Carrera S, *Acta Cryst*, 20 (1966) 783.

17 Birker J W L, Helder J, Henkel G, Krebs B & Reedjk, J, *lnorg Chem* 21 (1982) 357.
18 Kitano Y K, Ishitani A, Sato H, Imamura S & Ashida T, *Acta Crystallogr* C47 (1991) 1269.
19 Khan H, Badshah A, Shaheen F, Gieck C & Qureshi R A, *Acta Crystallogr* E64 (2008) o1141.
20 Stark J G & Wallace H G, Chemistry data book, John Murray: London, (1982) 31.
21 Bernstein J, Davis R E, Shimoni L & Chang N L, *Angew Chem Int Ed Engl*, 34 (1995) 1555.
22 Spackman M A & Jayatilaka D, *Cryst Eng Comm* 11 (2009) 19.
23 Turner M J, McKinnon J J, Jayatilaka D & Spackman M A, *Cryst Eng Comm*, 13 (2011) 1804.
24 Edwards A J, Mackenzie C F, Spackman P R, Jayatilaka D & Spackman M A, *Faraday Discussions*, 203 (2017) 93.
25 Turner M J, Thomas S P, Shi M W, Jayatilaka D & Spackman M A, *Chem Commun*, 51 (2015) 3735.
26 Mulliken R S, *J Chem Phys*, 23 (1955) 1833.
27 Fukui K, Yonezawa T, & Shingu H, *J Chem Phys*, 20 (1952) 722.
28 Lewis D F V, Ioannidis C, & Parke D V, *Xenobiotica*, 24 (1994) 401.